AEM
Journals.ASM.org

Polyhydroxyfullerene Binds Cadmium Ions and Alleviates Metal-Induced Oxidative Stress in *Saccharomyces cerevisiae*

Arunava Pradhan,[a] José Paulo Pinheiro,[b] Sahadevan Seena,[a] Cláudia Pascoal,[a] Fernanda Cássio[a]

Centre of Molecular and Environmental Biology, Department of Biology, University of Minho, Campus of Gualtar, Braga, Portugal[a]; Institute for Biotechnology and Bioengineering/Center for Molecular and Structural Biomedicine, Department of Chemistry and Biochemistry, Faculty of Sciences and Technology, University of Algarve, Campus of Gambelas, Faro, Portugal[b]

The water-soluble polyhydroxyfullerene (PHF) is a functionalized carbon nanomaterial with several industrial and commercial applications. There have been controversial reports on the toxicity and/or antioxidant properties of fullerenes and their derivatives. Conversely, metals have been recognized as toxic mainly due to their ability to induce oxidative stress in living organisms. We investigated the interactive effects of PHF and cadmium ions (Cd) on the model yeast *Saccharomyces cerevisiae* by exposing cells to Cd (≤5 mg liter^{-1}) in the absence or presence of PHF (≤500 mg liter^{-1}) at different pHs (5.8 to 6.8). In the absence of Cd, PHF stimulated yeast growth up to 10.4%. Cd inhibited growth up to 79.7%, induced intracellular accumulation of reactive oxygen species (ROS), and promoted plasma membrane disruption in a dose- and pH-dependent manner. The negative effects of Cd on growth were attenuated by the presence of PHF, and maximum growth recovery (53.8%) was obtained at the highest PHF concentration and pH. The coexposure to Cd and PHF decreased ROS accumulation up to 36.7% and membrane disruption up to 30.7% in a dose- and pH-dependent manner. Two mechanisms helped to explain the role of PHF in alleviating Cd toxicity to yeasts: PHF decreased Cd-induced oxidative stress and bound significant amounts of Cd in the extracellular medium, reducing its bioavailability to the cells.

Fullerene and functionalized fullerenes are carbon-based nanoparticles with enormous implications for nanotechnology due to their applications in several fields, such as biomedical diagnostics and therapeutics (1, 2) and remediation in wastewater treatment plants (3). However, some studies have reported potential toxicity and ecotoxicity of fullerene (4, 5), and consequently, fullerene was placed on the top of the Organisation for Economic Co-operation and Development (OECD) list (OECD guidance manual [6]) seeking toxicity tests and risk assessment. On the other hand, polyhydroxyfullerene (PHF), a functionalized derivative of fullerene, is in the limelight of current research due to its reported nontoxic nature and reactive oxygen species (ROS)-quenching properties (7, 8). PHF has an edge over fullerene in commercial and research applications because it is stable and soluble in aqueous solution due to the presence of hydroxyl groups. As an antioxidant agent and free radical scavenger, PHF has been reported to decrease the excitotoxic and apoptotic death of neurons (9), protect against ischemia-reperfused lungs (10), protect rat brain from alcoholic injury (11), prevent hepatotoxicity in rats and human cell lines (12), and decrease tumor size in rats (13). In contrast, cytotoxicity of PHF has also been observed (4, 14, 15). Under photoexcitation, PHF can generate free radical species (15) and induce early apoptosis and lipid peroxidation (14). These discrepant findings make it relevant to further assess the effects of PHF on biological systems.

Cadmium (Cd), a nonessential element for living organisms, has been used in various industrial and regular-life products, such as batteries, pigments and paints, alloys, and welding and electroplating materials, leading to its increased release in the environment (16). For instance, a quantitative estimation of Cd for Chinese rivers pointed to 4.45 tonnes (t) of Cd deposited per year along the Anhui section of the Yangtze River and to a high Cd content in the suspended matter (104.8 μg g^{-1}) in the Shun'an River (17). As a nonbiodegradable element, Cd has a very long biological half-life (18), and it has been reported to be toxic to macro- and microorganisms, including yeasts (19–21). Cd toxicity has been shown to be caused by oxidative stress (22, 23); Cd can indirectly generate free radicals by replacing iron or copper ions in cytoplasmic and membrane proteins, leading to an increase of free or chelated metals (23), which in turn can lead to oxidative stress via Fenton reactions (24, 25). ROS production was associated with Cd-induced cell death in rainbow trout (26), murine splenocytes (27), and human hepatoma cells (28). ROS triggered by Cd can react with several biomolecules within cells and may lead to DNA mutation, alterations in protein structure and function, lipid peroxidation, shifts in gene expression, and apoptosis (23, 29).

We investigated the potential role of PHF in alleviating Cd toxicity in yeasts under the hypothesis that (i) oxidative stress induced by Cd may be mitigated by PHF due to its antioxidant and free radical-scavenging properties and/or (ii) PHF may interact with Cd ions, reducing its bioavailability. We selected the yeast *Saccharomyces cerevisiae* because (i) it has been used as a eukaryotic model system to study oxidative stress responses (30–32) and (ii) mounting evidence suggests that Cd can induce oxidative stress by accumulating ROS or free radicals (22, 33, 34). Because the uptake and toxicity of Cd in yeasts can change with environmental conditions (e.g., pH [35] and Cd concentration [36]), we

Received 23 April 2014 **Accepted** 11 July 2014
Published ahead of print 18 July 2014
Editor: A. A. Brakhage
Address correspondence to Fernanda Cássio, fcassio@bio.uminho.pt.
Supplemental material for this article may be found at http://dx.doi.org/10.1128/AEM.01329-14.

doi:10.1128/AEM.01329-14

assessed the effects of Cd and PHF alone and in mixtures on yeast growth, intracellular ROS accumulation, and plasma membrane integrity at different pHs and exposure concentrations. Moreover, we used scanning electron microscopy coupled to an energy-dispersive X-ray analyzer (SEM-EDX) and scanned stripping chronopotentiometry (SSCP), a dynamic electrochemical stripping technique, to examine putative physicochemical interactions between PHF nanoparticles and Cd ions in an attempt to better understand the mode of action of these nanoparticles in biological systems.

MATERIALS AND METHODS

Preparation of Cd and PHF stocks. The stock solution of Cd (chloride salt, 98%; Sigma) was prepared in filtered ultrapure (Milli-Q) water (0.2-μm-pore-size membrane; Millipore, Billerica, MA) and stored at 4°C in the dark. The stock of PHF [$C_{60}(OH)_{18-22}$; BuckyUSA, Houston, TX] was prepared by suspending the powder in autoclaved (121°C, 20 min) ultrapure water, and the suspension was sonicated (42 kHz, 100 W; Branson 2510; Branson, Danbury, CT) for 10 min in the dark. A uniform aqueous suspension of PHF was obtained with no detectable precipitation after 3 weeks of storage at 4°C in the dark.

Yeast growth and exposure conditions. The yeast *Saccharomyces cerevisiae* PYCC 4072 was obtained from the Portuguese Yeast Culture Collection (New University of Lisbon, Portugal) and maintained on yeast peptone dextrose (YPD) solid medium with the following composition: dextrose (2%, wt/vol), peptone (1%, wt/vol), yeast extract (0.5%, wt/vol), and agar (2%, wt/vol). For the assays, cells grown on YPD agar (48 h at 26°C) were inoculated in YPD liquid medium.

Erlenmeyer flasks (100 ml) with 20 ml of YPD medium were supplemented with Cd (0, 1.5, or 5 mg liter^{-1}) and/or PHF (0, 50, 250, or 500 mg liter^{-1}), and the pH of the medium was adjusted to 5.8, 6.3, and 6.8. To assess the effects of PHF and Cd alone and in mixtures, exponentially growing cells (5×10^5 CFU ml^{-1}) in YPD medium were inoculated in each replicate flask and incubated with shaking (150 rpm) for 26 h at 26°C (12 chemical treatments × 3 pHs × 3 replicates, for a total of 108 flasks). To further clarify the antioxidant role of PHF, cell suspensions from the following cultures were prepared: (i) cells grown in YPD medium for 26 h at pH 6.3 without or with PHF and/or H_2O_2 and (ii) cells grown in YPD medium for 26 h at pH 6.3 without or with PHF, washed in PBS, and further exposed for 3 h to H_2O_2. Concentrations of PHF and H_2O_2 were 500 mg liter^{-1} and 10 mM, respectively. The yeast growth was monitored by spectrophotometry (optical density [OD] at 600 nm; UV-1700 PharmaSpec; Shimadzu, Kyoto, Japan).

Visualization of cell morphology by scanning electron microscopy. Yeast cells grown in YPD medium in the absence or presence of Cd and/or PHF were harvested (5,000 × *g*, 10 min; Sigma 113 centrifuge; Sigma, Germany), washed twice, and resuspended in 2 ml phosphate-buffered saline (1× PBS, pH 7.4; GIBCO). Cells were fixed in 2.5% (vol/vol) glutaraldehyde for 24 h and dehydrated in ethanol (vol/vol) as follows: 20%, 8 h; 40%, 6 h; 60%, 4 h; 80%, 2 h; and 100%, 1 h. Cell suspensions (20 μl) were then loaded on clean grease-free slides, coated with gold in a vacuum, and examined by scanning electron microscopy (SEM, Leica Cambridge S 360; Leica, Cambridge, United Kingdom) coupled to an energy-dispersive X-ray (EDX) microanalysis setup (15 keV).

Plasma membrane integrity and intracellular ROS accumulation assessed by flow cytometry and epifluorescence microscopy. Plasma membrane integrity was assessed by a membrane-impermeative dye, propidium iodide (PI; Molecular Probes, Eugene, OR), which enters the cells and binds to nucleic acids when plasma membrane disruption occurs; red fluorescence in cells indicates plasma membrane disruption (32). Nuclei were localized with 4′,6-diamidino-2-phenylindole dye (DAPI; Molecular Probes, Eugene, OR, USA), which forms a blue fluorescent complex with double-stranded DNA. Yeast cells were harvested and washed as described above, before being suspended in 2 ml PBS containing PI (20 μg ml^{-1}) and DAPI (0.1 mg ml^{-1}). The mixture was incubated for 15 min at 26°C in the dark.

Intracellular ROS accumulation was assessed with MitoTracker Red CM-H_2XRos (Molecular Probes, Eugene, OR). This dye does not fluoresce in the reduced form, but when it enters an actively respiring cell, it is oxidized by ROS in the mitochondria to form a red fluorescent compound (32, 37). Yeast cells, obtained as described above, were resuspended in 2 ml PBS containing 40 μg ml^{-1} of the dye prepared in dimethyl sulfoxide (≥99.9%; Sigma) and incubated for 15 min at 26°C in the dark.

For visualization of intracellular ROS accumulation and plasma membrane disruption, stained yeast suspensions were placed on a grease-free slide and mixed with an equal volume of an anti-fading and anti-photobleaching reagent (Vectashield mounting medium; Vector Laboratories, CA). Slides were scanned under an epifluorescence microscope (magnification ×1,000; Leica DM5000B; Leica, Germany), and a minimum of 3 arbitrary images per replicate were acquired with a digital camera (Leica DFC 350 FX R2) using the software LAS AF V1.4.1.

Quantitative fluorescence in yeast cells was measured using a flow cytometer (Epics XL-MCL; Beckman Coulter, Germany) equipped with an argon ion laser emitting a 488-nm beam at 15 mW. The red fluorescence of PI or MitoTracker Red was detected on an FL3 log filter through a 590-nm long pass, a 620-nm band pass, and another 670-nm long pass. An acquisition protocol was defined to measure forward scatter (FS log), side scatter (SS log), and red fluorescence (FL3 log) on a 4-decade logarithmic scale (32, 37). Each replicate was sampled three times, and 25,000 cells per sample were scanned. Data were analyzed with the software WinMDI 2.8. Cells exposed to 10 mM H_2O_2 served as positive controls (38).

Characterization of Cd and PHF nanoparticles alone or in mixtures. A stock aqueous suspension of PHF nanoparticles and YPD medium containing Cd and/or PHF were examined by SEM-EDX as described by Pradhan et al. (39). Briefly, 20 μl of each solution/suspension was loaded on a clean grease-free slide in the dark, air dried, and coated with gold in a vacuum. Slides were scanned by SEM-EDX as described above to confirm the presence of Cd or C in PHF nanoparticles.

The hydrodynamic size distribution of PHF nanoparticles was monitored by dynamic light scattering (DLS) to check agglomeration of nanoparticles in the stock suspension and in the YPD medium, using a Malvern Zetasizer Nano ZS (Malvern Instruments Limited, United Kingdom).

The behavior of binding of Cd to PHF was determined by SSCP (40). First, the binding of Cd to PHF was studied in 10 mM $NaNO_3$ (needed for electrochemical experiments) in the absence of YPD medium. Then, Cd binding to the medium was studied in the absence of PHF, and finally, the metal binding was studied with all components. Due to limitations of the upper detection limit of SSCP, the Cd at the highest exposure concentration was diluted 100×. To maintain exposure Cd-to-PHF ratios (1:10, 1:25, and 1:100), PHF and the YPD medium components were diluted by the same factor; i.e., assays were carried out in the presence or absence of YPD medium at a fixed Cd concentration (0.05 mg liter^{-1}) with either PHF concentration (0.5, 2.5, and 5.0 mg liter^{-1}) or pH (6.8, 6.3, and 5.8) being varied. For each set of experiments, the complex stability constants (K') and the diffusion coefficients of metal-ligand (Cd-PHF or Cd-YPD) complexes (D_{ML}) were determined based on the work of Pinheiro et al. (40) (see the supplemental material). Briefly, K' was determined from the potential shift, $\Delta E_{d,1/2}$, corrected for the decrease in transition time using an expression that is equivalent to the DeFord-Hume expression:

$$\ln(1 + K') = -(nF/RT)\Delta E_{d,1/2} - \ln(\tau^*_{M+L}/\tau^*_M) \quad (1)$$

$\Delta E_{d,1/2}$ is the SSCP shift of the half-wave potential (V), n is the number of electrons involved in the faradaic process, F is the Faraday constant (C mol^{-1}), R is the universal gas constant, T is the absolute temperature, and τ^*_{M+L} and τ^*_M are limiting transition times obtained in the presence and absence of the complexing ligand, respectively (40). The D_{ML} coefficient was computed from K' using the equation above and the mass balance for the metal:

TABLE 1 Metal-ligand complex stability constant (K') and particle diameter computed from the SSCP curves and recomputed for the exposure conditions of 5 mg liter^{-1} total Cd[a]

PHF (mg liter^{-1})	pH 5.8			pH 6.3			pH 6.8		
	K'	Diam (nm)	Estimated free Cd (mg liter^{-1})	K'	Diam (nm)	Estimated free Cd (mg liter^{-1})	K'	Diam (nm)	Estimated free Cd (mg liter^{-1})
Without YPD									
0									
50							27		
250							140	9	
500	80	8		165	8		271	9	
With YPD									
0	29		0.170	40		0.125	46		0.108
50							81	9	0.062
250							183	9	0.027
500	111	7	0.045	206	8	0.024	313	10	0.016

[a] Original data were obtained at 10 mM $NaNO_3$ and 0.05 mg liter^{-1} Cd ($C_{Cd,T} = 5 \times 10^{-7}$ M, or 0.05 mg liter^{-1}). The K' [$= K(C_{L,T}) = C_{ML}/C_M$] values were multiplied by a dilution factor of 100. C_{ML} and C_M are the concentrations of the metal-ligand complex (ML) and free metal (M), respectively, and $C_{L,T}$ corresponds to the total concentration of ligand, which was 100× higher in the exposure experiments.

$$D_{ML} = \bar{D} - \frac{1}{K'}(D_M - \bar{D}) \quad (2)$$

$\bar{D}$ is the mean diffusion coefficient of free metal (M) and its ligand complex (ML) in solution, and D_M is the diffusion coefficient of free metal in solution ($m^2\ s^{-1}$) (40). Free metal concentrations were estimated for the highest exposure concentration of Cd in the yeast assays (5×10^{-5} M; 5 mg liter^{-1}) using K' values for Cd binding to YPD medium and to PHF in the medium at different pH values.

Statistical analyses. Two-way analyses of variance (ANOVA) (41) were used to assess how yeast endpoints were affected by (i) PHF and pH at each Cd concentration and (ii) Cd and pH at each PHF concentration. Significant differences between treatments and respective controls or between pH values were analyzed by Bonferroni posttests (41). Data (as percentages) were arcsine square root transformed to achieve normal distribution and homoscedasticity (41). Analyses were done with Statistica 6.0 (Statsoft, Inc., Tulsa, OK).

RESULTS

Characterization of PHF nanoparticles. SEM analysis of PHF in the aqueous stock suspension showed two size ranges for spherical nanoparticles: 30 to 60 nm and 100 to 250 nm (data not shown). These results were confirmed by DLS, which yielded two peaks with mean particle sizes of 38.4 nm and 185.4 nm, corresponding to 32.4% and 0.1% of the number of mean size particles, respectively (see Table S1 in the supplemental material). In YPD medium, an additional peak with particle sizes ranging from 1.6 to 2.9 nm was found (peak 3; see Table S1). This was probably due to nanocrystal composites of the YPD medium, because a similar peak was observed in the absence of PHF (data not shown). In YPD medium, the mean size of PHF and polydispersity index (PdI) increased with the decrease in pH (peak 1, 43.6 versus 51.5 nm; peak 2, 198.3 versus 210.5 nm; PdI, 0.495 versus 0.597 [at pH 6.8 and 5.8, respectively]; see Table S1). Also, the relative abundance of smaller PHF nanoparticles was reduced by the decrease in pH of YPD medium (11.5% and 0.2% at pH 6.8 and pH 5.8, respectively; see Table S1). This suggests that nanoparticle agglomeration increased with decreasing pH.

SSCP yielded particle sizes from 7 to 10 nm (Table 1), obtained by applying the Stokes-Einstein equation to the diffusion coefficients, which ranged from 4×10^{-11} to 6×10^{-11} $m^2\ s^{-1}$. Particle size did not change much with PHF concentration and pH. Unfortunately, it was not possible to obtain the diameter for particles in the YPD medium due to the lower binding strength. It is known that DLS is severely biased toward larger sizes in polydisperse systems, and SEM analysis often does not detect smaller particles. On the other hand, SSCP is biased toward the smaller particles, which have a higher diffusion coefficient. Also, nanoparticle aggregation was less likely to occur at the lower concentration of PHF used in the SSCP assays.

Physicochemical interactions between PHF and Cd. The presence of PHF nanoparticles and Cd ions in YPD medium was confirmed by SEM-EDX (Fig. 1). A peak of C and an increased peak of O, compared to those in YPD medium without PHF, confirmed the presence of PHF nanoparticles in the medium (Fig. 1A and C versus B). YPD medium containing Cd showed peaks of this element (Fig. 1B). As expected, when the medium was supplemented with Cd and PHF, peaks of C, O, and Cd were detected (Fig. 1C). Under these conditions, instead of self-agglomeration, nanoparticles of PHF interacted with Cd by keeping this element arrested and surrounded by PHF nanoparticles, which formed crossed-links with other Cd crystals (Fig. 1C). A peak of Cl was also detected (Fig. 1B and C), because Cd was supplied as chloride salts. Additional elements detected in all samples (Fig. 1A to C) probably originated from glass slides and culture medium (Na, Mg, Si, Ca, and O) or gold coating (Au), because these elements were also found in the absence of PHF and Cd (data not shown).

SSCP analysis showed that in the absence of YPD, at pH 6.8, with a 10-fold excess of ligand (i.e., 5 mg liter^{-1} of Cd for 50 mg liter^{-1} of PHF), the complex stability constant was modest ($K' = 27$), indicating that most of the Cd was in its free form (Table 1; also, see Fig. S1 in the supplemental material). However, significant binding of Cd^{2+} by PHF was found at higher PHF concentrations (Table 1). The increase of K' to 140 and 271 at 250 and 500 mg liter^{-1} of PHF, respectively, suggested that the binding was homogeneous (i.e., a similar K' value would be obtained if divided by PHF concentration). A decrease in pH decreased the binding

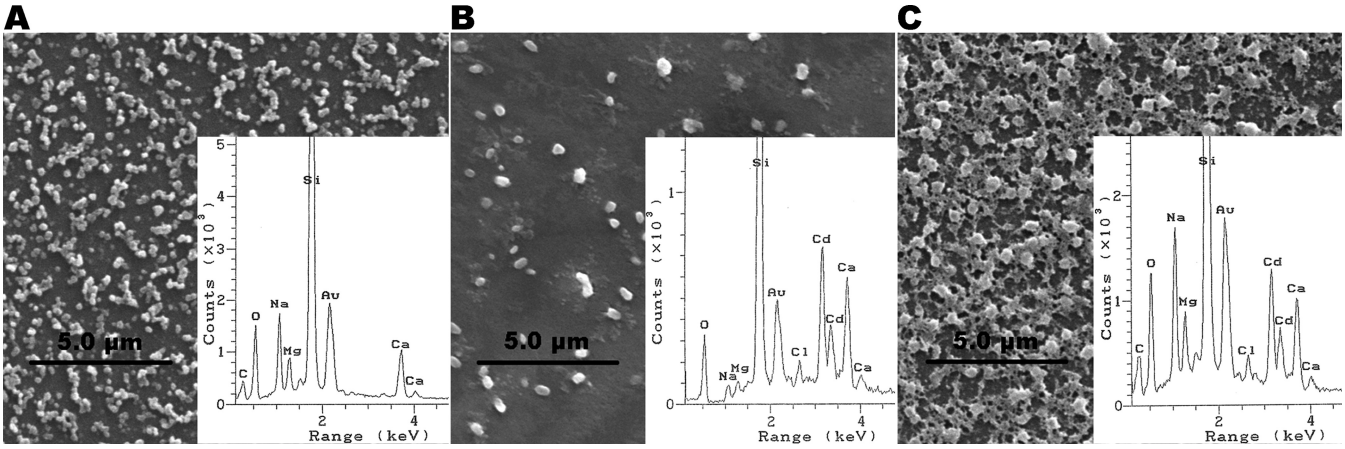

FIG 1 SEM and EDX (insets) microanalysis of YPD medium (pH 6.3) containing (A) 500 mg liter^{-1} PHF, (B) 5 mg liter^{-1} Cd, or (C) a mixture of 5 mg liter^{-1} Cd and 500 mg liter^{-1} PHF after 26 h of incubation at 26°C with shaking in the absence of yeast cells.

strength, as expected due to the smaller amounts of deprotonated groups in PHF.

The YPD medium could also bind Cd, but the binding was much lower than that promoted by high concentrations of PHF (Table 1). The SSCP waves with different dilutions of YPD medium indicated that the binding was homogeneous (see Fig. S2 in the supplemental material). The binding increased with pH (from 5.8 to 6.8), but varying the pH produced smaller effects than increasing the PHF concentration (Table 1). This indicates that the amount of deprotonated groups did not change much, especially between pH 6.3 and 6.8. Significant binding of Cd^{2+} in the YPD medium was obtained at the highest PHF concentration at pH 6.8 (Table 1; also, see Fig. S1C in the supplemental material). Again, Cd^{2+} binding decreased with decrease in pH (Table 1; also, see Fig. S1D). In the YPD medium, the free Cd concentration decreased with increase in pH and was roughly 30 to 50 times lower than the total Cd concentration (Table 1). Moreover, the K' values obtained were basically the sum of K' from the individual experiments, suggesting that the Cd binding by PHF and YPD medium was additive and resulted in a 10-fold decrease of free Cd at the highest pH and PHF concentration.

Effects of PHF and Cd on cell morphology and yeast growth. Compared to the control, the exposure of yeasts to PHF did not lead to morphological alterations in the cells, as shown by SEM (Fig. 2A). In contrast, the exposure to Cd induced remarkable morphological alterations, such as cell shrinkage and degeneration (Fig. 2A). The coexposure to Cd and PHF led to minor morphological alterations in just a few yeast cells (Fig. 2A).

In the absence of Cd and PHF, yeast growth was not affected by pHs between 5.8 and 6.8 ($P > 0.05$) (Fig. 2B). In the absence of Cd, PHF stimulated yeast growth ($P < 0.05$) (Fig. 2B). The exposure to 250 mg liter^{-1} of PHF increased yeast growth by 7.7% and 9.7% at pH 6.3 and 6.8, respectively ($P < 0.05$), while the exposure to the highest PHF concentration (500 mg liter^{-1}) stimulated yeast growth at all pHs (6.9% and 10.4% at pH 5.8 and 6.8, respectively; $P < 0.05$).

Exposure to Cd alone inhibited yeast growth, and the effects were stronger at higher pHs and Cd concentrations ($P < 0.05$); at pH 6.8, the growth was reduced to 64.5% at the lower Cd concentration and to 20.3% at the higher Cd concentration (Fig. 2B). The presence of PHF attenuated Cd inhibitory effects on yeast growth: Cd effects were less pronounced at higher PHF concentrations and pHs ($P < 0.05$) (Fig. 2B). Growth recovery from exposure to 1.5 mg liter^{-1} of Cd and 500 mg liter^{-1} of PHF was 28.4% at pH 6.8 (Fig. 2B). At this PHF concentration and pH, growth recovery from exposure to 5 mg liter^{-1} of Cd was 53.8%.

Effects of PHF and Cd on plasma membrane integrity. In the absence of PHF and Cd, yeast cells did not show plasma membrane disruption, as indicated by the absence of red fluorescence after PI staining under epifluorescence microscopy (Fig. 2C); under these conditions, cell nuclei were localized by the blue fluorescence after DAPI staining. Results from flow cytometry showed that the number of yeast cells with plasma membrane disruption was low (≤1.4%) at all tested pHs (Fig. 2D). The number of PI-positive cells decreased with increasing PHF concentration ($P < 0.05$) (Fig. 2D).

Cd led to plasma membrane disruption, as revealed by the presence of red fluorescence in cells (Fig. 2C), and the effects increased with increasing Cd concentration and pH ($P < 0.05$) (Fig. 2D). Exposure to 1.5 mg liter^{-1} of Cd led to 11.6% (pH 5.8) and 13.8% (pH 6.8) PI-positive cells, while exposure to the higher concentration of Cd increased the percent PI-positive cells to 34.7% and 38.1% at pH 5.8 and 6.8, respectively (Fig. 2D).

Plasma membrane disruption induced by Cd was reduced when yeast cells were coexposed to PHF, as shown by a decrease in red cell fluorescence (Fig. 2C). The level of plasma membrane disruption induced by Cd depended on PHF concentration and pH ($P < 0.05$) (Fig. 2C). The maximum reduction in the number of PI-positive cells was found after coexposure to the highest concentrations of PHF and Cd at the highest pH and corresponded to a decrease of 30.7% in PI-positive cells compared to cells exposed to Cd alone ($P < 0.05$) (Fig. 2D).

Effects of PHF and Cd on ROS accumulation. Epifluorescence microscopy analysis of yeast cells did not show ROS accumulation in the absence of Cd, as indicated by the absence of intense red fluorescence after MitoTracker Red CM-H_2XRos staining (Fig. 2E). Consistently, results from flow cytometry showed that less than 3.1% of cells unexposed to Cd had intracellular ROS accumulation at pHs ranging from 5.8 to 6.8 ($P < 0.05$) (Fig. 2F).

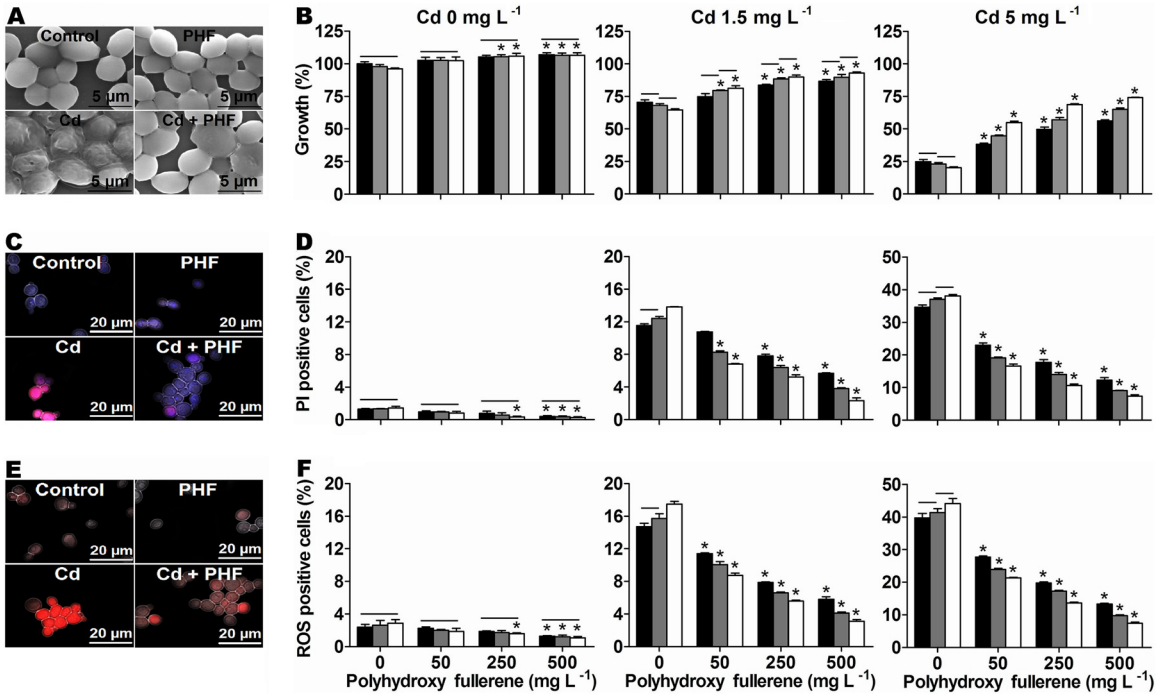

FIG 2 Qualitative effects of Cd (5 mg liter^{-1}) and/or PHF (500 mg liter^{-1}) on *S. cerevisiae* grown in YPD medium (pH 6.3) for 26 h. (A) Cell morphology assessed by scanning electron microscopy; (C) DAPI-stained nuclei (blue fluorescence) and plasma membrane disruption shown by red fluorescence after PI staining under an epifluorescence microscope; (E) intracellular ROS accumulation shown by red fluorescence after MitoTracker Red staining under an epifluorescence microscope. All fluorescent images were colocalized with respective bright fields. (B to F) Quantitative effects of increased concentrations of Cd and/or PHF at pH 5.8 (black bars), pH 6.3 (gray bars), and pH 6.8 (white bars) on (B) yeast growth, (D) plasma membrane disruption, assessed by flow cytometry after PI staining, and (F) intracellular ROS accumulation, assessed by flow cytometry after MitoTracker Red staining. Values are means and standard errors of the means ($n = 3$). Asterisks indicate results that differ significantly from control values ($P < 0.05$). A horizontal line indicates no significant difference between pH treatments.

Exposure to increasing PHF concentrations reduced ROS accumulation ($P < 0.05$) (Fig. 2F).

Exposure to Cd increased ROS accumulation in yeast cells (Fig. 2E) in a dose- and pH-dependent manner ($P < 0.05$) (Fig. 2F). The highest number of cells showing ROS accumulation (44.1%) was detected after exposure to 5 mg liter^{-1} of Cd at pH 6.8 (Fig. 2F). The presence of PHF diminished the accumulation of ROS induced by Cd (Fig. 2E); this mitigating effect increased with increasing PHF concentration and pH ($P < 0.05$) (Fig. 2F). The coexposure to the highest concentrations of PHF and Cd, at pH 6.8, led to 7.4% ROS-positive cells (Fig. 2F). This indicates that the presence of PHF decreased by up to 36.7% the number of cells with ROS accumulation induced by Cd.

Role of PHF in coping with oxidative stress in yeast cells. Exposure of yeast cells to H_2O_2 for 26 h at pH 6.3 (Table 2) led to a significant decrease in growth (21.5% of control; $P < 0.05$) which was accompanied by a strong increase in intracellular ROS accumulation (95% ROS-positive cells; $P < 0.05$). The coexposure of cells to H_2O_2 and PHF led to a significant growth recovery (68.1% of control) and to an attenuation of ROS accumulation (44.2% ROS-positive cells). Similar results were found when cells grown in the presence of PHF were subsequently exposed to H_2O_2 alone (Table 2), suggesting that PHF had the ability to cope with the oxidative stress generated by H_2O_2 inside cells.

DISCUSSION

Although cytotoxicity of the functionalized carbon nanomaterial PHF has been reported (4, 14, 15), several studies have highlighted its nontoxic nature and ROS-quenching properties in biological systems (7, 8, 12). We used the yeast *S. cerevisiae* as a eukaryotic model system to confirm that Cd induces oxidative stress (22, 23) and to provide the first insights into the mechanisms by which PHF is able to mitigate the stress induced by metals. Similarly to other authors (e.g., Oliveira et al. [36]), we found that Cd inhibited the growth of *S. cerevisiae* in a dose-dependent manner. In our study, the negative effects of Cd on yeast growth increased with pH from 5.8 to 6.8. This was surprising, because we found larger amounts of free Cd in the extracellular medium at the lower pH.

TABLE 2 Effects of PHF and H_2O_2 on yeast growth and intracellular ROS accumulation assessed by flow cytometry after MitoTracker Red staining[a]

Exposure conditions	% growth		% of cells exhibiting ROS	
	Grown in YPD only	Exposed to PBS + H_2O_2	Grown in YPD only	Exposed to PBS + H_2O_2
Control	100 ± 2.05 a	71.8 ± 1.53 a	3.1 ± 0.36 a	39.9 ± 0.2 a
PHF	109.0 ± 2.24 b	93.8 ± 1.1 b	0.66 ± 0.27 b	20 ± 0.46 b
H_2O_2	21.5 ± 0.01 c		95 ± 0.38 c	
PHF + H_2O_2	68.1 ± 3.78 d		44.17 ± 0.34 d	

[a] Cells were grown in YPD medium for 26 h at 26°C in the absence (control) or presence of PHF (500 mg liter^{-1}) and/or H_2O_2 (10 mM). A portion of the control cells or cells grown in the presence of PHF were washed in PBS and further exposed to H_2O_2 for 3 h in the same buffer. In each column, different letters indicate significant differences ($P < 0.05$).

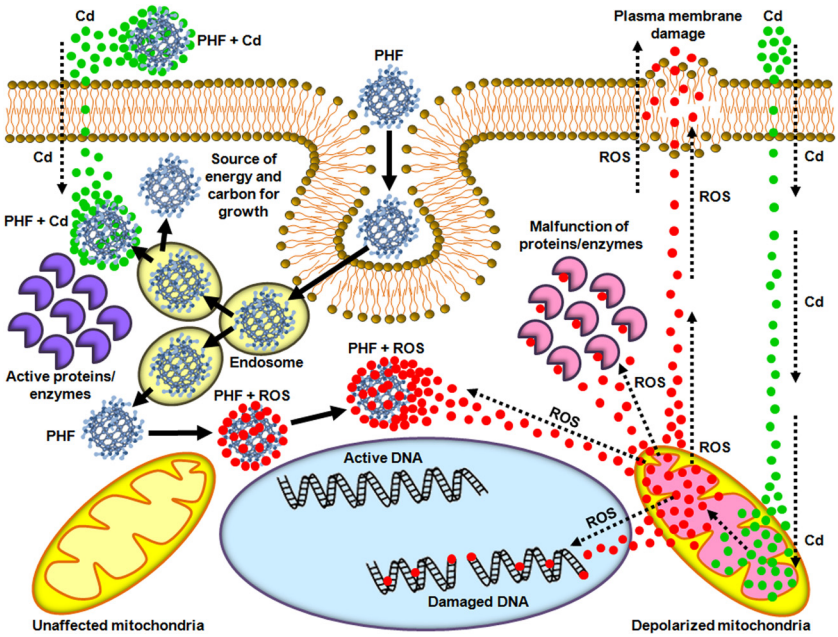

FIG 3 Schematic representation of possible modes of action of Cd (dashed arrows) and PHF (solid arrows) in yeast cells based on our results and the literature. Extracellular binding of Cd ions (green dots) to PHF decreases the concentration of bioavailable Cd (this study). The free Cd ions can enter the cell (54) and induce the accumulation of ROS (red dots) in active mitochondria, leading to mitochondrial depolarization, malfunction of proteins/enzymes, and nuclear and plasma membrane damage. PHF can enter the cell via the clathrin pathway (55), which is the mechanism of endocytosis identified in yeasts (56). PHF can be used as a source of energy or carbon in the absence of glucose (this study) and may also bind intracellular Cd and/or scavenge ROS, alleviating the cytotoxicity induced by Cd.

However, the affinity of protons for binding sites on the yeast is much higher than that of metal ions at lower pH, and the uptake of Cd by this yeast is reported to be ca. 2 times higher at pH 6.0 than 5.0 (35). Therefore, the increase in Cd toxicity with pH in our study might be related to pH-dependent Cd uptake by the yeast.

Cd leads to oxidative injury in cells of living organisms due to intracellular accumulation of ROS (in microbes [19, 20], plants [21], animals [22, 23], and humans [28]). Consistently, we found that Cd induced ROS accumulation and plasma membrane disruption in cells of *S. cerevisiae* in a dose-dependent manner. The more pronounced effects of Cd on plasma membrane integrity and ROS accumulation at higher pHs may be related to the effects of pH on the magnitude of metal uptake by the cells (see above). Moreover, the results suggest that not all cells with ROS accumulation had lost their membrane integrity, because the number of cells with plasma membrane disruption (PI-positive cells) was slightly lower than that of ROS-positive cells, with differences of up to 6.1% at pH 6.8.

The exact mechanism of Cd toxicity is not fully understood yet, but most probably, Cd cytotoxicity is the combination of (i) apoptosis resulting from increased ROS accumulation saturating the antioxidant system, with mitochondrial membrane depolarization and dysfunction, and (ii) membrane lipid peroxidation promoted by ROS accumulation, which leads to plasma membrane permeabilization and necrosis (42–45). Our findings support the idea that Cd toxicity for *S. cerevisiae* was related to oxidative stress via intracellular ROS accumulation and/or via plasma membrane disruption, which might be due to lipid peroxidation. In addition, SEM analysis showed that Cd induced alterations of cell morphology, with evidence of cell shrinkage and degeneration. Thus, overall Cd-mediated toxicity might have involved apoptotic and/or necrotic cell death of *S. cerevisiae*. However, further studies are still needed to clarify this.

In the absence of Cd, PHF stimulated the growth of *S. cerevisiae*; this agrees with studies reporting that these nanoparticles can be beneficial for the growth of some prokaryotic (46) and eukaryotic organisms, including fungi (47). White rot fungi are capable of mineralizing PHF to CO_2 and of incorporating minor amounts of C from PHF into lipid biomass (48). We also found that PHF nanoparticles can be used as the sole carbon source by *S. cerevisiae*; however, yeast growth was almost 7-fold lower in mineral medium with vitamins and oligoelements supplemented with PHF (200 mg liter^{-1}) than in YPD medium (20 mg liter^{-1} of dextrose) (data not shown). These findings contrast the reported harmful effects of other nanoparticles, including fullerene, on biota (4, 39, 49, 50).

In our study, the coexposure of *S. cerevisiae* to PHF nanoparticles and Cd decreased the number of cells with (i) intracellular ROS accumulation, (ii) plasma membrane disruption, and (iii) altered morphology, compared to cells exposed to Cd alone. These effects were consistent with the attenuated negative effects of Cd on yeast growth in the presence of PHF. Moreover, the ability of PHF to mitigate Cd toxicity increased with nanoparticle concentration. In our study, PHF was able to cope with the oxidative stress generated by H_2O_2, supporting the idea that these nanoparticles can protect yeasts against metal-induced oxidative stress. By reducing the levels of intracellular ROS, PHF may stabilize mitochondrial membrane potential and prevent mitochondrial dysfunction (2, 51), a common manifestation of Cd-induced oxidative stress that leads to apoptosis. Also, PHF can prevent oxidation of polyunsaturated fatty acid in liposomes (mimic of plasma membrane) and lipid peroxidation (52). However, the mecha-

nisms underlying the antioxidant properties of PHF nanoparticles are still unclear. Đorđević and Bogdanović (53) explained the PHF antioxidant properties by two possible mechanisms: (i) an addition reaction of hydroxyl radicals (·OH, 2n) to the olefinic double bonds of PHF core and/or (ii) removal of a hydrogen from PHF by the hydroxyl radical.

Complementarily to the antioxidant role of PHF, electrochemical stripping analyses showed extracellular binding of Cd to PHF in a concentration- and pH-dependent manner that led to a reduction in the concentration of bioavailable Cd. The binding effects of PHF in the presence of YPD medium suggested that the binding was additive. Cd binding by PHF resulted in up to a 10-fold decrease of free Cd, which translated into a significant protection against Cd toxicity. Also, SEM-EDX analysis showed that Cd ions were surrounded by PHF nanoparticles, supporting the idea that the functionalized surface hydroxyl groups of PHF could trap Cd while still having a facet available for interacting with yeast cells. In addition, the more pronounced decrease in Cd toxicity promoted by PHF at higher pHs was probably due to greater availability of unbound and/or nonaggregated PHF nanoparticles with unmasked hydroxyl groups to interact with Cd ions, as disclosed by the shift toward smaller nanoparticles and lower PdIs at higher pHs (see Table S1 in the supplemental material). These results provided the mechanistic explanation for the alleviating effects of PHF on Cd-induced cytotoxicity. Thus, along with hydroxyl radicals or ROS-scavenging properties, PHF directly interacted with Cd, and pH was a key factor for the stability and availability of PHF nanoparticles to the yeast cells. Figure 3 schematically summarizes the possible modes of action of Cd and PHF in yeast cells based on our results and data from literature.

In conclusion, this study provided the first mechanistic evidence that PHF nanoparticles can play a role against metal toxicity in biological systems. The results show that PHF nanoparticles mitigated Cd effects by protecting cells against oxidative stress, as revealed by a decrease in intracellular ROS accumulation and in the number of cells with altered morphology and plasma membrane disruption. The protective role of PHF against Cd stress was dose dependent, and effects were more pronounced at elevated pHs. In the absence of Cd, the stimulatory effect of PHF on yeast growth supported the idea that PHF nanoparticles can be used as carbon and/or energy sources. The results also indicated that PHF nanoparticles bound significant amounts of Cd, reducing the bioavailability of Cd to yeast cells, particularly at elevated PHF concentrations and pHs. The ability of PHF nanoparticles to interact with metals opens new perspectives for the development of remediation strategies.

ACKNOWLEDGMENTS

FEDER-POFC-COMPETE and the Portuguese Foundation for Science and Technology (PEst-OE/BIA/UI4050/2014, PTDC/AAC-AMB/121650/2010) supported this work and A.P. (SFRH/BD/45614/2008). J.P.P. acknowledges the financial support of Pest-OE/EQB/LA0023/2013.

We are grateful to A. Pacheco for helping with flow cytometry.

REFERENCES

1. **Bosi S, Da Ros T, Spalluto G, Prato M.** 2003. Fullerene derivatives: an attractive tool for biological applications. Eur. J. Med. Chem. **38:**913–923. http://dx.doi.org/10.1016/j.ejmech.2003.09.005.
2. **Partha R, Conyers JL.** 2009. Biomedical applications of functionalized fullerene-based nanomaterials. Int. J. Nanomed. **4:**261–275. http://dx.doi.org/10.2217/nnm.09.11.
3. **Anderson R, Barron AR.** 2005. Reaction of hydroxyfullerene with metal salts: a route to remediation and immobilization. J. Am. Chem. Soc. **127:**10458–10459. http://dx.doi.org/10.1021/ja051659d.
4. **Sayes CM, Fortner JD, Guo W, Lyon D, Boyd AM, Ausman KD, Tao YJ, Sitharaman B, Wilson LJ, Hughes JB, West JL, Colvin VL.** 2004. The differential cytotoxicity of water-soluble fullerenes. Nano Lett. **4:**1881–1887. http://dx.doi.org/10.1021/nl0489586.
5. **Oberdörster E, Zhu S, Blickley TM, McClellan-Green P, Haasch ML.** 2006. Ecotoxicology of carbon-based engineered nanoparticles: effects of fullerene (C_{60}) on aquatic organisms. Carbon **44:**1112–1120. http://dx.doi.org/10.1016/j.carbon.2005.11.008.
6. **Organisation for Economic Co-operation and Development (OECD).** 2010. Guidance manual for the testing of manufactured nanomaterials: OECD's sponsorship programme, ENV/JM/MONO(2009)20REV. OECD environment, health and safety publications, series on the safety of manufactured nanomaterials, no. 25. Organisation for Economic Co-operation and Development, Paris, France.
7. **Lai HS, Chen WJ, Chiang LY.** 2000. Free radical scavenging activity of fullerenol on the ischemia-reperfusion intestine in dogs. World J. Surg. **24:**450–454. http://dx.doi.org/10.1007/s002689910071.
8. **Vávrová J, Řezáčová M, Pejchal J.** 2012. Fullerene nanoparticles and their anti-oxidative effects: a comparison to other radioprotective agents. J. Appl. Biomed. **10:**1–8. http://dx.doi.org/10.2478/v10136-012-0002-2.
9. **Dugan LL, Gabrielsen JK, Yu SP, Lin TS, Choi DW.** 1996. Buckminsterfullerenol free radical scavengers reduce excitotoxic and apoptotic death of cultured cortical neurons. Neurobiol. Dis. **3:**129–135. http://dx.doi.org/10.1006/nbdi.1996.0013.
10. **Chen YW, Hwang KC, Yen CC, Lai YL.** 2004. Fullerene derivatives protect against oxidative stress in RAW 264.7 cells and ischemia-reperfused lungs. Am. J. Physiol. Regul. Integr. Comp. Physiol. **287:**R21–R26. http://dx.doi.org/10.1152/ajpregu.00310.2003.
11. **Tykhomyrov AA, Nedzvetsky VS, Klochkov VK, Andrievsky GV.** 2008. Nanostructures of hydrated C_{60} fullerene (C_{60}HyFn) protect rat brain against alcohol impact and attenuate behavioral impairments of alcoholized animals. Toxicology **246:**158–165. http://dx.doi.org/10.1016/j.tox.2008.01.005.
12. **Injac R, Perse M, Obermajer N, Djordjevic-Milic V, Prijatelj M, Djordjevic A, Cerar A, Strukelj B.** 2008. Potential hepatoprotective effects of fullerenol $C_{60}(OH)_{24}$ in doxorubicin-induced hepatotoxicity in rats with mammary carcinomas. Biomaterials **29:**3451–3460. http://dx.doi.org/10.1016/j.biomaterials.2008.04.048.
13. **Krishna V, Singh A, Sharma P, Iwakuma N, Wang Q, Zhang Q, Knapik J, Jiang H, Grobmyer SR, Koopman B, Moudgil B.** 2010. Polyhydroxy fullerenes for non-invasive cancer imaging and therapy. Small **6:**2236–2241. http://dx.doi.org/10.1002/smll.201000847.
14. **Johnson-Lyles DN, Peifley K, Lockett S, Neun BW, Hansen M, Clogston J, Stern ST, McNeil SE.** 2010. Fullerenol cytotoxicity in kidney cells is associated with cytoskeleton disruption, autophagic vacuole accumulation, and mitochondrial dysfunction. Toxicol. Appl. Pharmacol. **248:**249–258. http://dx.doi.org/10.1016/j.taap.2010.08.008.
15. **Wielgus AR, Zhao B, Chignell CF, Hu DN, Roberts JE.** 2010. Photototoxicity and cytotoxicity of fullerol in human retinal pigment epithelial cells. Toxicol. App. Pharmacol. **242:**79–90. http://dx.doi.org/10.1016/j.taap.2009.09.021.
16. **Ayres RU.** 1992. Toxic heavy metals: materials cycle optimization. Proc. Natl. Acad. Sci. U. S. A. **89:**815–820. http://dx.doi.org/10.1073/pnas.89.3.815.
17. **Zhao CD, Chen FR, Chen XR, Zhao HC, Xia WL, Nie HF, Kong M, Liu F, Yang K.** 2008. Methodology of tracking source of cadmium anomalies and their quantitative estimation in the Yangtze River basin. Earth Sci. Front. **15:**179–194. http://dx.doi.org/10.1016/S1872-5791(09)60004-X.
18. **Sugita M, Tsuchiya K.** 1995. Estimation of variation among individuals of biological half-time of cadmium calculated from accumulation data. Environ. Res. **68:**31–37. http://dx.doi.org/10.1006/enrs.1995.1005.
19. **Chen T, Li W, Schulz PJ, Furst A, Chien PK.** 1995. Induction of peroxisome proliferation and increase of catalase activity in yeast, Candida albicans, by cadmium. Biol. Trace Elem. Res. **50:**125–133. http://dx.doi.org/10.1007/BF02789415.
20. **Choi J.** 2009. Adsorption, bioavailability, and toxicity of cadmium to soil microorganisms. Geomicrobiol. J. **26:**248–255. http://dx.doi.org/10.1080/08827500902892077.
21. **Vestena S, Cambraia J, Ribeiro C, Oliveira JA, Oliva MA.** 2011. Cadmium-induced oxidative stress and antioxidative enzyme response in wa-

ter hyacinth and salvinia. Braz. J. Plant Physiol. **23:**131–139. http://dx.doi.org/10.1590/S1677-04202011000200005.
22. **Brennan RJ, Schiestl RH.** 1996. Cadmium is an inducer of oxidative stress in yeast. Mutat. Res. **356:**171–178. http://dx.doi.org/10.1016/0027-5107(96)00051-6.
23. **Valko M, Rhodes CJ, Moncol J, Izakovic M, Mazur M.** 2006. Free radicals, metals and antioxidants in oxidative stress-induced cancer. Chem. Biol. Interact. **160:**1–40. http://dx.doi.org/10.1016/j.cbi.2005.12.009.
24. **Price DJ, Joshi JG.** 1983. Ferritin. Binding of beryllium and other divalent metal ions. J. Biol. Chem. **258:**10873–10880.
25. **Casalino E, Sblano C, Landriscina C.** 1997. Enzyme activity alteration by cadmium administration to rats: the possibility of iron involvement in lipid peroxidation. Arch. Biochem. Biophys. **346:**171–179. http://dx.doi.org/10.1006/abbi.1997.0197.
26. **Risso-de Faverney C, Orsini N, de Sousa G, Rahmani R.** 2004. Cadmium-induced apoptosis through the mitochondrial pathway in rainbow trout hepatocytes: involvement of oxidative stress. Aquat. Toxicol. **69:**247–258. http://dx.doi.org/10.1016/j.aquatox.2004.05.011.
27. **Pathak N, Khandelwal S.** 2006. Oxidative stress and apoptotic changes in murine splenocytes exposed to cadmium. Toxicology **220:**26–36. http://dx.doi.org/10.1016/j.tox.2005.11.027.
28. **Oh SH, Lim SC.** 2006. A rapid and transient ROS generation by cadmium triggers apoptosis via caspase-dependent pathway in HepG2 cells and this is inhibited through N-acetylcysteine-mediated catalase upregulation. Toxicol. Appl. Pharmacol. **212:**212–223. http://dx.doi.org/10.1016/j.taap.2005.07.018.
29. **Wang L, Xu T, Lei WW, Liu DM, Li YJ, Xuan RJ, Ma JJ.** 2011. Cadmium-induced oxidative stress and apoptotic changes in the testis of freshwater crab, *Sinopotamon henanense*. PLoS One **6:**e27853. http://dx.doi.org/10.1371/journal.pone.0027853.
30. **Priault M, Camougrand N, Kinnally KW, Vallette FM, Manon S.** 2003. Yeast as a tool to study Bax/mitochondrial interactions in cell death. FEMS Yeast Res. **4:**15–27. http://dx.doi.org/10.1016/S1567-1356(03)00143-0.
31. **Landolfo S, Politi H, Angelozzi D, Mannazzu I.** 2008. ROS accumulation and oxidative damage to cell structures in *Saccharomyces cerevisiae* wine strains during fermentation of high-sugar-containing medium. Biochim. Biophys. Acta **1780:**892–898. http://dx.doi.org/10.1016/j.bbagen.2008.03.008.
32. **Mendes-Ferreira A, Sampaio-Marques B, Barbosa C, Rodrigues F, Costa V, Mendes-Faia A, Ludovico P, Leão C.** 2010. Accumulation of non-superoxide anion reactive oxygen species mediates nitrogen-limited alcoholic fermentation by *Saccharomyces cerevisiae*. Appl. Environ. Microbiol. **76:**7918–7924. http://dx.doi.org/10.1128/AEM.01535-10.
33. **Liu J, Zhang Y, Huang D, Song G.** 2005. Cadmium induced MTs synthesis via oxidative stress in yeast *Saccharomyces cerevisiae*. Mol. Cell Biochem. **280:**139–145. http://dx.doi.org/10.1007/s11010-005-8541-4.
34. **Muthukumar K, Nachiappan V.** 2010. Cadmium-induced oxidative stress in *Saccharomyces cerevisiae*. Indian J. Biochem. Biophys. **47:**383–387.
35. **Mapolelo M, Torto N.** 2004. Trace enrichment of metal ions in aquatic environments by *Saccharomyces cerevisiae*. Talanta **64:**39–47. http://dx.doi.org/10.1016/j.talanta.2003.10.058.
36. **Oliveira RP, Basso LC, Junior AP, Penna TC, Del Borghi M, Converti A.** 2012. Response of *Saccharomyces cerevisiae* to cadmium and nickel stress: the use of the sugar cane vinasse as a potential mitigator. Biol. Trace Elem. Res. **145:**71–80. http://dx.doi.org/10.1007/s12011-011-9156-0.
37. **Ludovico P, Rodrigues F, Almeida A, Silva MT, Barrientos A, Côrte-Real M.** 2002. Cytochrome c release and mitochondria involvement in programmed cell death induced by acetic acid in *Saccharomyces cerevisiae*. Mol. Biol. Cell **13:**2598–2606. http://dx.doi.org/10.1091/mbc.E01-12-0161.
38. **Belenky P, Camacho D, Collins JJ.** 2013. Fungicidal drugs induce a common oxidative-damage cellular death pathway. Cell Rep. **3:**350–358. http://dx.doi.org/10.1016/j.celrep.2012.12.021.
39. **Pradhan A, Seena S, Pascoal C, Cássio F.** 2011. Can metal nanoparticles be a threat to microbial decomposers of plant litter in streams? Microb. Ecol. **62:**58–68. http://dx.doi.org/10.1007/s00248-011-9861-4.
40. **Pinheiro JP, Domingos R, Lopez R, Brayner R, Fiévet F, Wilkinson K.** 2007. Determination of diffusion coefficients of nanoparticles and humic substances using scanning stripping chronopotentiometry (SSCP). Colloids Surf. A Physicochem. Eng. Asp. **295:**200–208. http://dx.doi.org/10.1016/j.colsurfa.2006.08.054.
41. **Zar JH.** 2010. Biostatistical analysis, 5th ed. Prentice Hall, Upper Saddle River, NJ.
42. **Howlett NG, Avery SV.** 1997. Relationship between cadmium sensitivity and degree of plasma membrane fatty acid unsaturation in *Saccharomyces cerevisiae*. Appl. Microbiol. Biotechnol. **48:**539–345. http://dx.doi.org/10.1007/s002530051093.
43. **Sokolova MI, Evans S, Hughes FM.** 2004. Cadmium-induced apoptosis in oyster hemocytes involves disturbance of cellular energy balance but no mitochondrial permeability transition. J. Exp. Biol. **207:**3369–3380. http://dx.doi.org/10.1242/jeb.01152.
44. **López E, Arce C, Oset-Gasque MJ, Cañadas S, González MP.** 2006. Cadmium induces reactive oxygen species generation and lipid peroxidation in cortical neurons in culture. Free Radic. Biol. Med. **40:**940–951. http://dx.doi.org/10.1016/j.freeradbiomed.2005.10.062.
45. **Kroemer G, Galluzzi L, Brenner C.** 2007. Mitochondrial membrane permeabilization in cell death. Physiol. Rev. **87:**99–163. http://dx.doi.org/10.1152/physrev.00013.2006.
46. **Huang F, Ge L, Zhang B, Wang Y, Tian H, Zhao L, He Y, Zhang X.** 2014. A fullerene colloidal suspension stimulates the growth and denitrification ability of wastewater treatment sludge-derived bacteria. Chemosphere http://dx.doi.org/10.1016/j.chemosphere.2014.02.042.
47. **Gao J, Wang Y, Folta KM, Krishna V, Bai W, Indeglia P, Georgieva A, Nakamura H, Koopman B, Moudgil B.** 2011. Polyhydroxy fullerenes (fullerols or fullerenols): beneficial effects on growth and lifespan in diverse biological models. PLoS One **6:**e19976. http://dx.doi.org/10.1371/journal.pone.0019976.
48. **Schreiner KM, Filley TR, Blanchette RA, Bowen BB, Bolskar RD, Hockaday WC, Masiello CA, Raebiger JW.** 2009. White-rot basidiomycete-mediated decomposition of C_{60} fullerol. Environ. Sci. Technol. **43:**3162–3168. http://dx.doi.org/10.1021/es801873q.
49. **Handy RD, Owen R, Valsami-Jones E.** 2008. The ecotoxicology of nanoparticles and nanomaterials: current status, knowledge gaps, challenges, and future needs. Ecotoxicology **17:**315–325. http://dx.doi.org/10.1007/s10646-008-0206-0.
50. **Pradhan A, Seena S, Pascoal C, Cássio F.** 2012. Copper oxide nanoparticles can induce toxicity to the freshwater shredder *Allogamus ligonifer*. Chemosphere **89:**1142–1150. http://dx.doi.org/10.1016/j.chemosphere.2012.06.001.
51. **Cai X, Jia H, Liu Z, Hou B, Luo C, Feng Z, Li W, Liu J.** 2008. Polyhydroxylated fullerene derivative $C_{60}(OH)_{24}$ prevents mitochondrial dysfunction and oxidative damage in an MPP^+-induced cellular model of Parkinson's disease. J. Neurosci. Res. **86:**3622–3634. http://dx.doi.org/10.1002/jnr.21805.
52. **Mirkov SM, Djordjevic AN, Andric NL, Andric SA, Kostic TS, Bogdanovic GM, Vojinovic-Miloradov MB, Kovacevic RZ.** 2004. Nitric oxide-scavenging activity of polyhydroxylated fullerenol, $C_{60}(OH)_{24}$. Nitric Oxide **11:**201–207. http://dx.doi.org/10.1016/j.niox.2004.08.003.
53. **Đorđević A, Bogdanović G.** 2008. Fullerenol—a new nanopharmaceutic? Arch. Oncol. **16:**42–45. http://dx.doi.org/10.2298/AOO0804042D.
54. **Blackwell KJ, Singleton I, Tobin JM.** 1995. Metal cation uptake by yeast: a review. Appl. Microbiol. Biotechnol. **43:**579–584. http://dx.doi.org/10.1007/BF00164757.
55. **Li W, Chen C, Ye C, Wei T, Zhao Y, Lao F, Chen Z, Meng H, Gao Y, Yuan H, Xing G, Zhao F, Chai Z, Zhang X, Yang F, Han D, Tang X, Zhang Y.** 2008. The translocation of fullerenic nanoparticles into lysosome via the pathway of clathrin-mediated endocytosis. Nanotechnology **19:**145102. http://dx.doi.org/10.1088/0957-4484/19/14/145102.
56. **Weinberg J, Drubin DG.** 2012. Clathrin-mediated endocytosis in budding yeast. Trends Cell Biol. **22:**1–13. http://dx.doi.org/10.1016/j.tcb.2011.09.001.